# Fast imaging of intermittent electrospraying of water with positive corona discharge

**B Pongrác[1,2], H H Kim[2], M Janda[1], V Martišovitš[1] and Z Machala[1]**

[1] Division of Environmental Physics, Faculty of Mathematics, Physics and Informatics, Comenius University, Slovakia
[2] Institute for Environmental Management Technology, AIST, Japan

E-mail: branislav.pongrac@gmail.com

## Abstract

The effect of the electrospraying of water in combination with a positive direct current (dc) streamer corona discharge generated in air was investigated in this paper. We employed high-speed camera visualizations and oscilloscopic discharge current measurements in combination with an intensified charge-coupled device camera for fast time-resolved imaging. The repetitive process of Taylor cone formation and droplet formation from the mass fragments of water during the electrospray was visualized. Depending on the applied voltage, the following intermittent modes of electrospraying typical for water were observed: dripping mode, spindle mode, and oscillating-spindle mode. The observed electrospraying modes were repetitive with a frequency of a few hundreds of Hz, as measured from the fast image sequences. This frequency agreed well with the frequency of the measured streamer current pulses. The presence of filamentary streamer discharges at relatively low voltages probably prevented the establishment of a continuous electrospray in the cone–jet mode. After each streamer, a positive glow corona discharge was established on the water filament tip, and it propagated from the stressed electrode along with the water filament elongation. The results show a reciprocal character of intermittent electrospraying of water, and the presence of corona discharge, where both the electrospray and the discharge affect each other. The generation of a corona discharge from the water cone depended on the repetitive process of the cone formation. Also, the propagation and curvature of the water filament were influenced by the discharge and its resultant space charge. Furthermore, these phenomena were partially influenced by the water conductivity.

Keywords: electrospray, dc corona discharge, high-speed camera, fast iCCD imaging

(Some figures may appear in colour only in the online journal)

## 1. Introduction

The electrohydrodynamic (EHD) spray of liquids (sometimes also referred to as EHD atomization, EHDA, here simply called electrospray) has been a subject of research since the beginning of the last century. The pioneering works conducted by Zeleny in 1914 and 1917 [1, 2] were the first published experimental studies in this field, and were followed by others. Later, in 1964, another important study was conducted by Taylor, who first derived the condition for stable liquid cone existence [3]. Since then, electrospray became the subject of extensive studies by many researchers [4–10].

Generally, the electrospraying effect can be explained as follows. When the liquid medium (in our case water) flowing through the capillary (or nozzle) is not subjected to electrical stress, regular droplets with rounded shapes are formed from the end of the capillary. In this situation, the droplet size is given by the balance of capillary and gravitational forces. However, with the application of an electrical potential on the capillary, electric forces take effect. The effective surface tension of the liquid starts to decrease due to the presence of the electric field causing charge separation inside the liquid, and the volume of the forming droplets decreases. The charges of the polarity of the capillary move towards the droplet surface and induce a surface charge density, causing an increase of electrostatic pressure against the capillary pressure. When a critical voltage is reached, the shape of the droplet changes

J. Phys. D: Appl. Phys. **47** (2014) 315202

B Pongrác *et al*

to conical, which is referred to as a Taylor cone [3]. Under these conditions, there has to be a hydrostatic balance between the capillary pressure and the normal electric pressure at the conical surface of the liquid. Subsequently, a jet emerges from the tip of the Taylor cone and breaks into droplets due to the axisymmetric (varicose), lateral (kink), or ramified instabilities [8, 11]. These charged droplets are then accelerated by the electric field; Coulomb repulsion takes effect between them and finally the electrospray occurs. The droplets may further explode if the charge they carry exceeds the Rayleigh limit for instability, which is given by [12, 13]:

$$q_R = 8\pi\sqrt{\varepsilon_0\gamma r^3}, \tag{1}$$

where $q_R$ is the charge on the droplet, $\gamma$ is the surface tension of the liquid, and $r$ is the radius of the droplet. During electrospray, the size of the droplets can vary from tens of nm up to hundreds of $\mu$m [14, 15].

The above described process is specifically known as a cone–jet mode of electrospraying. This mode is typical for its relative stability and monodispersity (equal size) of droplets and is very often used in various applications [16–18]. However, observing this mode in atmospheric air for liquids with a higher surface tension (e.g. water) is not easy, since the critical electric field $E_c$ at the meniscus surface required to form this mode is proportional to the square root of the liquid surface tension $\gamma$ [15]:

$$E_c \sim \sqrt{\left(\frac{\gamma}{\varepsilon_0 R_j}\right)}, \tag{2}$$

where $R_j$ is the jet radius in this case, which depends on both the flow rate and the electrical conductivity of the liquid. Therefore, the necessary voltage for cone–jet mode generation can be higher than the electrical breakdown threshold of the surrounding gas. In this situation, a disruptive electric discharge can ensue and prevent this mode [15, 16, 19].

Depending on various parameters, several other modes of electrospraying can be generated (e.g. intermittent dripping and spindle modes, simple jet modes). These modes are pretty well described in [20, 21]. It is possible to generate these modes in water, too.

One of the recently introduced potential applications of water electrospray is the decontamination of water polluted with organic and microbial pollutants. It is interesting to use the effect of water electrospraying in combination with the discharge (e.g. streamer corona). In such cases, the water flows directly through the high-voltage (HV) needle electrode into the active discharge region, where it is sprayed into small droplets. The presence of the electrical discharge generating non-thermal plasma in the spraying area allows for very efficient mass transfer of plasma-generated species into water [22–24]. In this regard, it is necessary to better investigate the effect of electrospraying in combination with the discharge under various conditions.

Of course, there have been a few studies dealing with a discharge in the presence of the electrospray. In 1914, Zeleny studied the electrical discharge from the liquid points in his pioneering experiments [1, 25]. Later, in 1948, English investigated the corona discharge from a water drop and he was the first to present interesting results on the difference in positive and negative onset potentials [26]. In later years, this topic was approached by various scientists who contributed considerably to this area [27–32].

The present work aims to investigate the effect of the electrospraying of water in combination with positive direct current (dc) corona discharge. Generally, the discharge has a significant effect on the electrospray behaviour, as was partially explored in previous research. Recently, with the technological advances in optical and electrical measurement techniques and devices, there are new possibilities for the investigation of such complex and fast phenomena. The advantage of these methods is the capability of time-resolved visualization of fast phenomena, such as electrospray and discharge dynamics. Our main objective was to identify various modes of water electrospraying combined with corona discharge by high-speed (HS) camera, and to supplement these measurements with records of the discharge generation and propagation during the electrospray process by iCCD camera, photomultiplier tube (PMT) responses, and oscilloscopic current measurements.

## 2. Experimental set-up

The experimental set-up for investigations of electrospraying with dc corona discharge is shown in figure 1. The electrodes were a cylindrical hollow blunt needle anode (spraying nozzle) opposite to the mesh cathode, where both were stainless steel with the inter-electrode gap $d = 1$ cm. The inner and outer diameters (i.d. and o.d.) of the nozzles were 0.6 mm and 0.8 mm, respectively, for iCCD imaging, and 0.5 mm and 0.7 mm, respectively, for the HS camera visualization. The water was continuously supplied to the nozzle by a syringe pump NE-300 with a flow rate 0.4 ml min$^{-1}$ during HS camera measurements, or 0.5 ml min$^{-1}$ for iCCD measurements. The minor differences in the nozzle diameters and water flow rates for HS and iCCD camera measurements were caused by using slightly different experimental set-ups during the different experiments, and had a negligible effect on the electrospray behaviour. As a liquid, either deionized water with low conductivity (2 $\mu$S cm$^{-1}$) or NaCl water solution with higher conductivities (up to 4500 $\mu$S cm$^{-1}$) were used. The conductivities of the water solutions were measured using a conductivity meter (Mettler Toledo).

A positive dc discharge was generated by applying a HV from a dc power supply through a ballast resistor R (20 M$\Omega$) on the nozzle electrode. The discharge voltage was measured by a HV probe, Tektronix P6015A. The discharge current was measured on a 50 $\Omega$ resistor shunt. The current and voltage signals were processed by a digitizing oscilloscope, Tektronix TDS 2024 (200 MHz).

Optical visualization was used as the main method for the investigations of the electrospray phenomena. We used an HS camera Photron FASTCAM SA KH5, with the following settings kept for all HS measurements: the shutter exposure time 1 $\mu$s, resolution of 384 × 1024 pixels with 10 000 fps (frames per second). For studying the dynamic processes with a discharge, time-resolved imaging in combination with the oscilloscopic measurements of current pulses was employed.

J. Phys. D: Appl. Phys. **47** (2014) 315202

B Pongrác *et al*
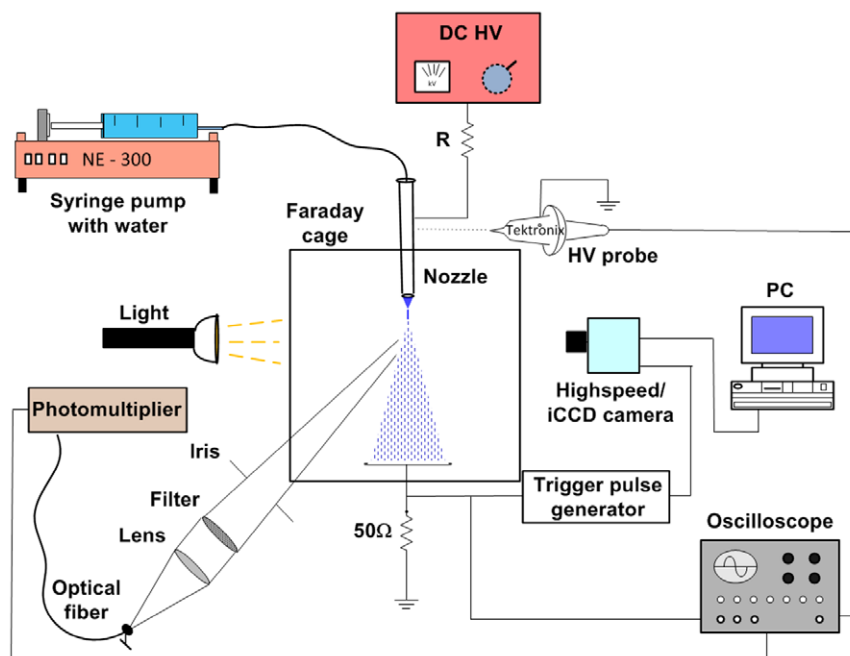


**Figure 1.** Experimental set-up for investigations of the electrospray of water, with a HV hollow needle (nozzle) electrode enabling water flow into the inter-electrode space.
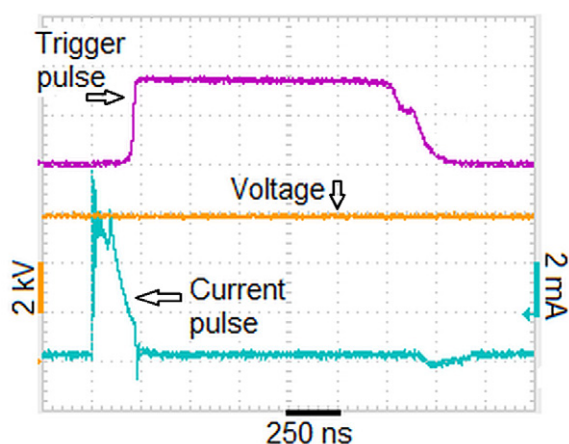


**Figure 2.** Oscilloscopic records of the discharge voltage and current pulse, and the pulse triggering the iCCD camera during the electrospraying of water.

For this purpose we used an iCCD camera, Andor iStar, with a minimum exposure time of 2 ns, and a maximum resolution of $1024 \times 1024$ pixels. The camera was externally triggered by a pulse generator that was triggered by the discharge current pulses with the peak current set only above 6 mA (figure 2), due to its technical limitation. The iCCD trigger pulses are delayed by several tens of nanoseconds with respect to the triggering current pulses, depending on the slope of the leading edge of the triggering current pulse. As a focusing and zooming optical system, a zoom lens Nikon (105 mm $f$/2.8 D Micro-Nikkor) and Nikon (105 mm $f$/2.8 G VR Micro-Nikkor) were attached to the iCCD camera and HS camera, respectively.

The main difference between the HS and the iCCD camera is that the HS camera can record the sequence of one unique droplet propagation (event) in a relatively short exposure time ($\mu$s), while the iCCD camera can detect this single event in an

even shorter time (ns), but the sequence of droplet propagation is constructed from the different repetitive events.

In order to link the current pulses with the propagation of the discharge, we used oscilloscopic measurements of current pulses in combination with a fast (2 ns rise time) and highly sensitive PMT Hamamatsu R955 (with a spectral response from 160 to 900 nm with maximum response at 400 nm), that is able to detect the very weak optical emissions of plasma (such as corona discharge). The entire plasma emission was measured either spectrally unresolved, or by using a narrow bandpass interference filter (Melles Griot 03 FIU127) transparent around 337.1 nm (with wavelength tolerance +3/−0 nm) to filter the emission of the $N_2$ (C–B, 0–0) transition only.

## 3. Results and discussion

### 3.1. Imaging of the electrospray modes

In our experimental set-up we observed a typical behaviour of droplet formation at the tip of the nozzle and its deformation with the applied electric field. Some modes of electrospraying described in the literature were observed [20, 21, 33]. In this configuration (1 cm gap, 0.4–0.5 ml min$^{-1}$ water flow rate), no stable modes (e.g. cone–jet modes) with the water filament constantly connected to the nozzle were observed. Only intermittent modes were present, with the water filament repetitively detaching from the nozzle. This can be explained by the relatively high surface tension and conductivity of water. In general, water is not a suitable liquid for stable electrospraying due to its high surface tension, although some papers show that stable jet modes of water were generated in longer gaps and higher flow rates [20, 33, 34].

With applying the voltage on the HV nozzle, the ejected droplets progressively decreased in size and the dripping mode

J. Phys. D: Appl. Phys. **47** (2014) 315202

B Pongrác *et al*
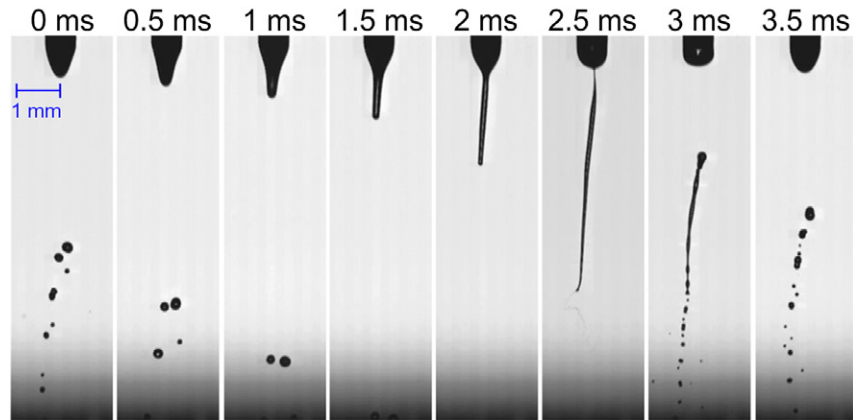


**Figure 3.** HS camera sequence of electrospraying of deionized water in spindle mode (6 kV, conductivity $2\,\mu\mathrm{S\,cm^{-1}}$, gap 1 cm, nozzle 0.7 mm o.d., 0.5 mm i.d., water flow rate $0.4\,\mathrm{ml\,min^{-1}}$, time step $500\,\mu\mathrm{s}$).

with no current pulses was observed first. During this mode, the voltage was not sufficient to deform the surface of the water droplet into the conical shape, and regular droplets with spherical shape were formed.

At the voltage ($U$) of about 4.5 kV, the character of the spraying changed and the Taylor cone was periodically formed at the tip of the nozzle. The dripping mode switched to a different mode, described in the literature as the spindle mode [20, 21, 33], accompanied by the appearance of the current pulses. With increasing voltage, the frequency of the current pulses usually increased during this mode. Figure 3 shows the sequence of HS camera images and demonstrates the electrospraying in the spindle mode at voltage 6 kV using deionized water with conductivity of $2\,\mu\mathrm{S\,cm^{-1}}$. These images represent different stages of one electrospraying event, starting from the Taylor cone formation, continuing through the elongation of the water filament, its detachment and eventual disintegration to small droplets, until the Taylor cone of the next electrospraying event starts to form. This process is repetitive and the period of the cone or droplet formation, calculated from several cycles of the HS camera sequence, is approximately 3.8 ms. It is in very good agreement with the average repetition frequency of the current pulses simultaneously measured by the oscilloscope (~260 Hz, figure 5).

At first, a cone is formed from the volume of water meniscus and it is gradually elongated in a direction towards the plane electrode. After some time, it is detached as an elongated fragment of bulk water. This elongation was more significant for deionized water, compared with a higher water conductivity. For higher conductivity, the detached water filament was significantly shorter and the mode was similar to the dripping mode. This difference could be caused by the effect of different tangential components of the electric field and the resultant tangential shear stress on the water surface, which causes the stabilization and elongation of the jet. The intensity of tangential electric field $E_\mathrm{t}$ is inversely proportional to the liquid conductivity $K$ and proportional to the current $i$ flowing through the cone–jet:

$$E_\mathrm{t} \approx \frac{i}{\pi K R_j^2}. \qquad (3)$$

Thus, the filament is longer for water with a lower conductivity. This effect was investigated and described in more detail elsewhere [34].

After the detachment of the fragment of water, it disrupts into several small droplets of different sizes, and the meniscus is contracted back to the nozzle. For higher conductivity, this fragment is significantly shorter and usually disrupts into two bigger droplets. Next, the formation of a new Taylor cone starts and the whole process repeats.

With changing some parameters (voltage, water conductivity), the character of the spraying changed and a new mode was observed. As shown in figure 4, for higher water conductivity $400\,\mu\mathrm{S\,cm^{-1}}$, the droplet generation was similar to the previous spindle mode, but the cone formation shifted from one side of the nozzle to another, and the elongated water fragments were no longer perpendicular to the plane electrode. Since the previously generated droplets are still close to the capillary outlet, the field generated by them can deflect the next jet off the capillary axis [21]. Similar to the spindle mode, this elongation of the water filament was more significant for deionized water with lower conductivity. After the filament detached from one side of the nozzle, it disintegrated into several droplets. Then a new cone started to form from the opposite side of the nozzle. When observed by the naked eye, this gives a visual impression of two well distinguished water streams. The average mode repetition frequency based on the HS camera imaging was about 315 Hz. It is again in relatively good agreement with the average frequency of current pulses measured electrically (~335 Hz). This mode looks like the oscillating-spindle mode and is similar to the mode observed by Jaworek and Krupa, called the multi-spindle mode therein [21].

In this experimental configuration, further increases of voltage usually led back to the spindle mode, and eventually to unstable intermittent modes with a variable repetition frequency until sparking occurred, which completely disrupted the electrospray process.

Basically, the water meniscus can also be considered as an HV liquid electrode with some defined curvature. Since the shape of the meniscus and the curvature vary during filament propagation, the electric field near the water meniscus tip changes locally, too. Generally, with the increasing curvature
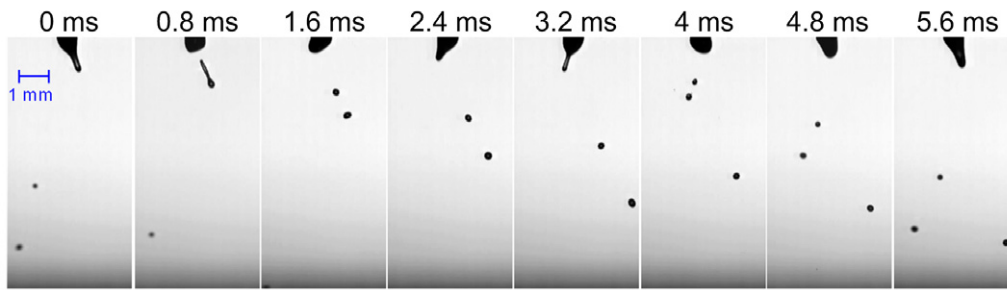
**Figure 4.** HS camera sequence of electrospraying of water in oscillating-spindle mode (6 kV, conductivity $400\,\mu S\,cm^{-1}$, gap 1 cm, nozzle 0.7 mm o.d., 0.5 mm i.d., water flow rate $0.4\,ml\,min^{-1}$, time step $800\,\mu s$).

of the meniscus tip, the intensity of the electric field should increase. This effect can have an influence on the streamer generation (section 3.4).

### 3.2. Measurements of the droplet size and time of flight

The fast camera image sequences also enabled us to estimate the average time of flight (time between the water filament disintegration and the droplet falling on the grounded electrode) in a 1 cm gap, and the sizes of the sprayed water droplets between the electrodes. For instance, in the case of low conductivity water ($2\,\mu S\,cm^{-1}$) shown in figure 3, the average time of flight is $\sim 100\,\mu s$ for the first incoming droplets from the head of the filament, and $\sim 2.5$ ms for the last one. The characteristic size of the water droplet (approximating to a spherical shape) varies from approximately $<10\,\mu m$ to $\sim 250\,\mu m$ in diameter. As can be seen from figures 4, 10 and 11, the droplet size becomes larger with higher liquid conductivities (from $\sim 190\,\mu m$ to $\sim 280\,\mu m$ for $400\,\mu S\,cm^{-1}$). The same applies to the time of flight which becomes longer (from $\sim 2.7$ ms to $\sim 6.3$ ms for $400\,\mu S\,cm^{-1}$). Since the droplets are formed by disintegration of the thin water filament, the sizes of the droplets are determined by the filament's thickness. The time of flight is related to the velocity of filament propagation and its length before disintegration. Both of these parameters (filament size and filament velocity) depend on water conductivity, as also described elsewhere [34].

Knowing the typical droplet size and time of flight is important in water decontamination applications when considering the mass transfer of plasma-generated active species into the water droplets while they are sprayed through the discharge. Our results on the bio-decontamination of water in a streamer corona or transient spark showed that even such short times of flight enable the efficient mass transfer of air plasma-generated reactive oxygen and nitrogen species in the sprayed water to induce significant bactericidal effects [22, 23]. In addition, water activated by the electrospray with very low flow rates ($\sim 0.05\,ml\,min^{-1}$) demonstrated enhanced bactericidal effects when sprayed on surfaces [24]. The key is probably in the very high surface to volume ratio of the droplets.

### 3.3. Relation between the current pulses and the mode repetition

Electrical discharges in the environment with liquid droplets have not been fully understood. The main objective of

this work was to investigate the mutual influence of the corona discharge and water electrospraying. We therefore tried to identify the sources of various current pulses in our electrospraying measurements, which should be generated mainly by the discharge phenomena. The oscilloscopic waveform showing the repetitive pulses can be seen in figure 5. These repetitive phenomena correspond to the spindle mode electrospraying shown in figure 3. Figure 5(b) shows the current pulses in the low time resolution of 2 ms/div. Figure 5(a) shows one current pulse in the high time resolution of 100 ns/div. From these records we calculated the average frequency of the current pulses.

Hypothetically, the observed pulses could be related to the individual charged droplets accelerated by the electric field. However, the number of observed droplets greatly exceeded the number of measured current pulses. As can be seen in figures 3 and 4, for every cycle of the Taylor cone formation (corresponding to the mode repetition frequency), two or more droplets are created (so the hypothetical frequency of current pulses originating from every droplet should be at least two times higher than that of the measured current pulses). Since the mode repetition frequency was in relatively good agreement with the frequency of current pulses, this hypothesis seems to be unlikely. Moreover, the measured current pulses had relatively high amplitudes (a few mA) typical for streamers [35], and the frequency of current pulses was in good agreement with the mode repetition frequency, as demonstrated in figures 6 and 7. In these figures, the combination of iCCD and HS camera measurements, taken simultaneously with oscilloscopic measurements for various water conductivities are shown. Only electrospray modes are included therein, with relatively stable periodicities for many cycles of Taylor cone formation. The filled red circles and black triangles represent the mode repetition frequencies measured by HS camera and iCCD camera, respectively. The open markers (circles and triangles) are data from the corresponding oscilloscopic measurements, and represent frequencies of the current pulses measured during imaging. It is possible to see a relatively good correlation between both of these frequencies (filled versus open markers). The current pulses are therefore more likely to be related to the pulsed character of the discharge itself. However, by the naked eye the visual impression of the discharge resembles the presence of a positive glow corona (sometimes also called Hermstein's glow) that is apparently pulseless for our current measurement sensitivity [36].

J. Phys. D: Appl. Phys. **47** (2014) 315202

B Pongrác *et al*
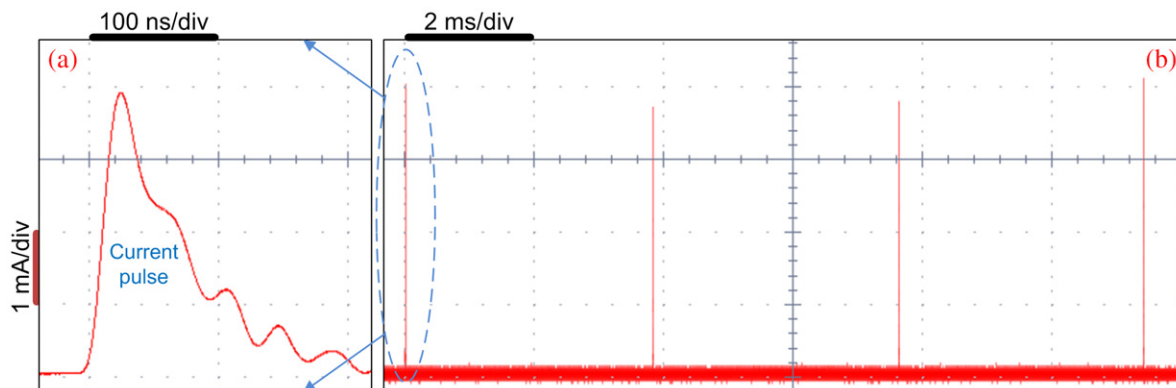


**Figure 5.** Oscilloscopic waveform of the discharge current pulses during the electrospraying of water in spindle mode. Image (*a*) corresponds to one current pulse in high time resolution 100 ns/div, image (*b*) corresponds to the many current pulses in low time resolution 2 ms/div (6 kV, conductivity 2 $\mu$S cm$^{-1}$, gap 1 cm, nozzle 0.7 mm o.d., 0.5 mm i.d., water flow rate 0.4 ml min$^{-1}$).
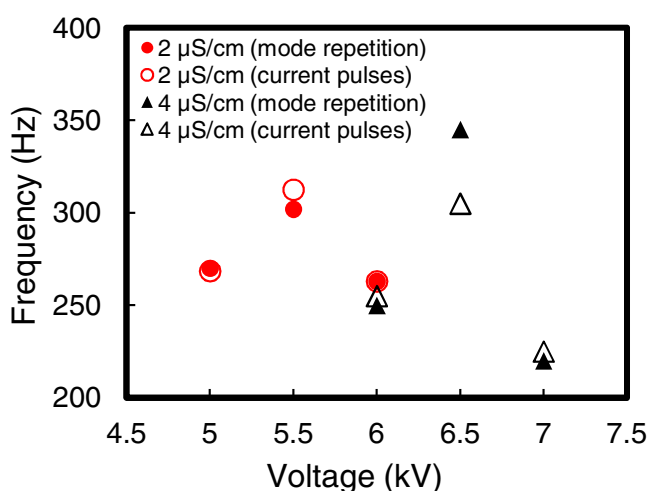


**Figure 6.** Comparison of mode repetition (filled markers) frequencies measured by HS or iCCD camera and the frequencies of current pulses (open markers) for various voltages and low water conductivities.
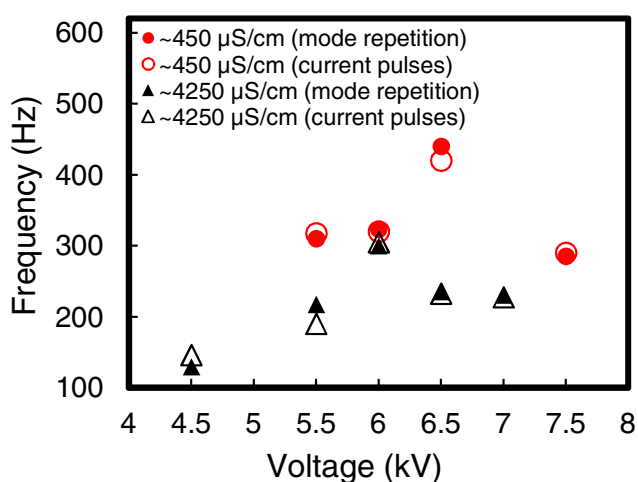


**Figure 7.** Comparison of mode repetition (filled markers) frequencies measured by HS or iCCD camera and the frequencies of current pulses (open markers) for various voltages and water solutions of high conductivities.

The discharge observed by the naked eye started at a voltage of 4.5 kV, together with current pulses with amplitudes of a few mA. At higher voltages (depending on water conductivity) it eventually transformed to spark. Phenomena of different breakdown voltages in dependence of water conductivity are investigated in more details in our other paper [34].

As can be seen from figures 6 and 7, for the given conductivity, the frequencies varied with the voltage, with transition from one electrospray mode to another: from the spindle mode to the oscillating-spindle mode where the frequency was usually higher, and then back into the spindle mode. Since the data shown were obtained by many measurements, some differences could be also caused by different conditions. However, the main purpose of these graphs is to show the good correlation between mode repetition frequencies measured by the HS and iCCD cameras and the frequencies of the current pulses measured oscilloscopically.

### 3.4. Corona discharge during the electrospray

The results in the preceding section show that the current pulses are most likely generated by pulsed discharge phenomena rather than by the charges transported by the droplets. In order to prove the correlation between the measured current pulses and the discharge, we used the synchronized measurements of the current and the light emitted by the discharge, which was detected by a PMT. The light signal was collected from the focal point located a few millimeters below the nozzle. The parameters of electrospraying during this measurement were almost the same as in figure 3, but the water conductivity was 500 $\mu$S cm$^{-1}$. Figure 8 shows oscilloscopic records of both current and PMT signals. The current pulse is followed by the emitted light pulse, with a delay of about 25 ns. After the subtraction of the PMT charge build-up time, and the signal transmission delay due to the BNC cables, the time difference between these two signals shortens to only 4 ns. The two signals always occurred together and the frequencies of both pulses were equal. This observation supported our assumption that the current pulses are generated by a discharge with a pulsed character.

The different widths of the photomultiplier pulse and the current pulse can be explained by different durations of these

J. Phys. D: Appl. Phys. **47** (2014) 315202

B Pongrác *et al*
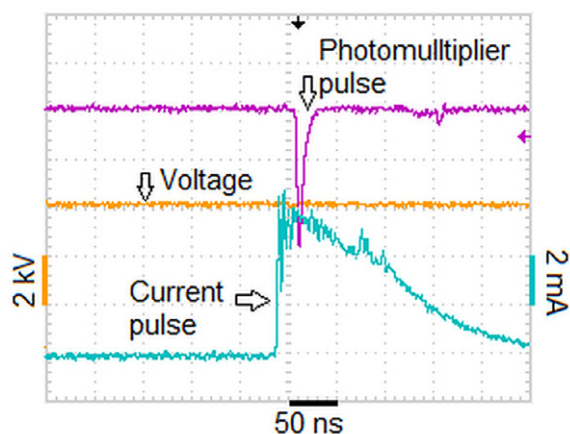


**Figure 8.** Oscilloscopic records of the discharge voltage, current pulse, and the PMT pulse (6 kV, conductivity 500 $\mu$S cm$^{-1}$ gap 1 cm, nozzle 0.8 mm o.d., 0.6 mm i.d.).

two phenomena. Current waveform is most likely given by the drift of electrons and ions in the electric field which can be estimated from the Shockley-Ramo theorem. The light emission is mostly produced by the excited species created by energetic electrons impact during the formation of avalanches and streamers in the initial phase of the current signal (rising slope) when the electric field in the streamer head is still sufficiently high. The phase of deexcitation occurs in very short time (1–10 ns) and corresponds to the duration of the light emission. Later, as the streamer propagates along the gap, the electric field decreases in its head, the current and the energy of electrons decrease too, and the plasma gets into the decay phase where electrons do not have enough energy to produce more excited species, however, they still drift to the anode and contribute to the current signal. This is why the emission signal is spiked and narrower than the current signal. Since the light emission signal was collected from the focal point located a few millimeters below the nozzle, this difference could be more significant.

Considering that the pulse is generated by a discharge, it should be possible to detect the light emission of the discharge by iCCD camera. For this purpose we used the iCCD camera that was triggered by the discharge current pulse itself (figure 1). Thanks to the good regularity and repetitiveness of the droplet formation, it was possible to construct a sequence of images similar to the HS camera sequence shown in figure 3. Let us note, however, that in iCCD camera imaging, every single image is related to the formation process of a different droplet.

Figures 9–11 show the iCCD images of spindle modes at voltage 6 kV using three different conductivities (4 $\mu$S cm$^{-1}$, 500 $\mu$S cm$^{-1}$ and 4500 $\mu$S cm$^{-1}$), respectively. For each illuminated image with droplets, the corresponding dark image of the discharge emission without illumination is shown. During these measurements, the gain function (related to light intensification) of the iCCD camera was adjusted differently for illuminated and dark images to reach a proper visualization. The exposure time was 10 $\mu$s for the illuminated (no light intensification) and 100 $\mu$s for the dark images (maximum light intensification), respectively. The only exception is the left

column 0 with dark images where the exposure time was 5 s (no light intensification), representing an integrated emission over this long period, with many droplet formation cycles.

The camera delay was gradually increased to the point where the image was approximately the same as the first one in the sequence (the droplet was at the same position). At this point, the next electrospraying event starts (column 4). These images represent different stages of the electrospraying event and the discharge propagation from 0 to 3, 3.5 and 4 ms (columns 1–4). The characteristic frequencies of these modes can be also seen in figures 6 and 7. Thanks to these combined sequences, it is possible to see the propagation of the discharge in relation to the water cone formation and propagation. For all three conductivities shown, the glow corona is first visible at the tip of the water cone (column 1). The water cone gradually elongates and creates the filament (also visible in figure 3). As the water filament propagates axially towards the grounded electrode, the bright spot of the glow corona remains present at the tip of this filament and propagates with it (column 2).

Although intuitively expected, we did not observe any corona discharge originating directly from the nozzle in the range of the studied (pre-breakdown) voltages (4.5–7 kV) in the 1 cm gap. This is demonstrated in figures 9–11, too, where the edges of the nozzle are shown with no light emission. Unlike in some of our other bio-decontamination studies [22, 23], the nozzle used here was a blunt hollow needle and so higher voltages would be needed to initiate the corona discharge on its edges. On the contrary, the sequences of dark images in figures 9–11, as well as the integrated emission in column 0, clearly demonstrate light emission of the glow corona discharge at the tip of the Taylor cone and the propagating water filament, eventually terminated with a filamentary discharge occurring in each cycle of droplet formation.

We observed the glow corona originating from the pointed filament tip even for the lowest water conductivities, despite the filament of water of such low conductivity representing a significant electrical resistance (as much as 5 M$\Omega$ for ~1 mm long Taylor cone of 4 $\mu$S cm$^{-1}$ water seen in figure 9, column 1, and as much as 55 M$\Omega$ for ~2.8 mm elongated thin filament seen in figure 9, column 2). The electrical resistances of the water filaments were estimated by using the Pouillet's law. However, the currents in the glow corona regime are low (~$\mu$A), so the voltage drop across the filament remains too low to completely suppress the enhancement of the electric field around the tip, and formation of the corona (~10 V in figure 9, column 1; up to max 150 V in the most extreme case in figure 9, column 2). The voltage drops across the water filaments were estimated by using the Ohms's law.

The appearance of this corona on the water filament tip is primarily the electric field effect. However, a closer look at this tip indicates how the ionic space charge resulting from the corona seems to affect the surface electric field at the filament and the shape of its tip (figures 9–11 illuminated images in column 2). A similar effect was observed and described by Borra *et al*, and Kuroda and Horiuchi [14, 28]. In highly conductive liquids, the liquid acts as a conductor and does not impose a significant voltage drop. The discharge
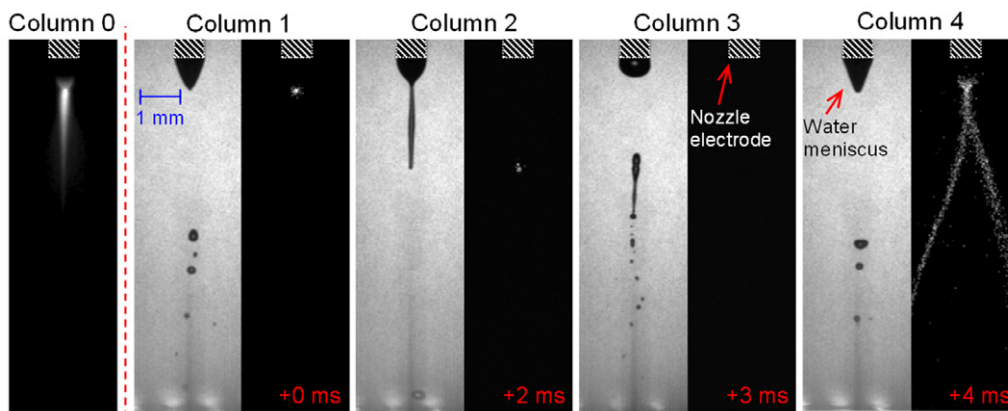
**Figure 9.** iCCD time sequence images of electrospraying of water (illuminated, columns 1–4 with exposure time 10 $\mu$s) with corona discharge (dark, columns 1–4 with exposure time 100 $\mu$s) in spindle mode for water conductivity 4 $\mu$S cm$^{-1}$, +6 kV, gap 1 cm, nozzle 0.8 mm o.d. and 0.6 mm i.d. iCCD dark images in column 0 with exposure time 5 s represent an integrated emission over the long period with many droplet formation cycles.
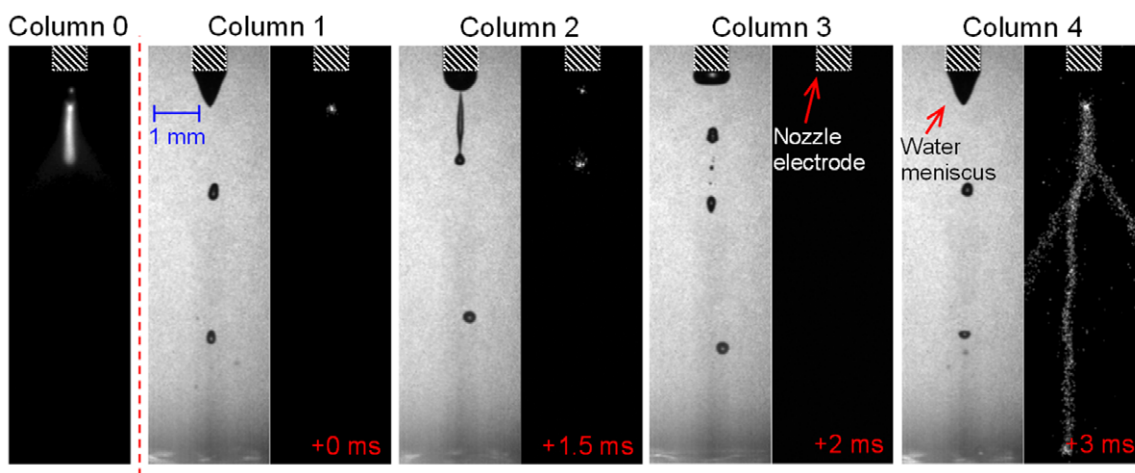


**Figure 10.** iCCD time sequence images of electrospraying of water (illuminated, columns 1–4 with exposure time 10 $\mu$s) with corona discharge (dark, columns 1–4 with exposure time 100 $\mu$s) in spindle mode for water conductivity 500 $\mu$S cm$^{-1}$, + 6 kV, gap 1 cm, nozzle 0.8 mm o.d. and 0.6 mm i.d. iCCD dark images in column 0 with exposure time 5 s represent an integrated emission over the long period with many droplet formation cycles.
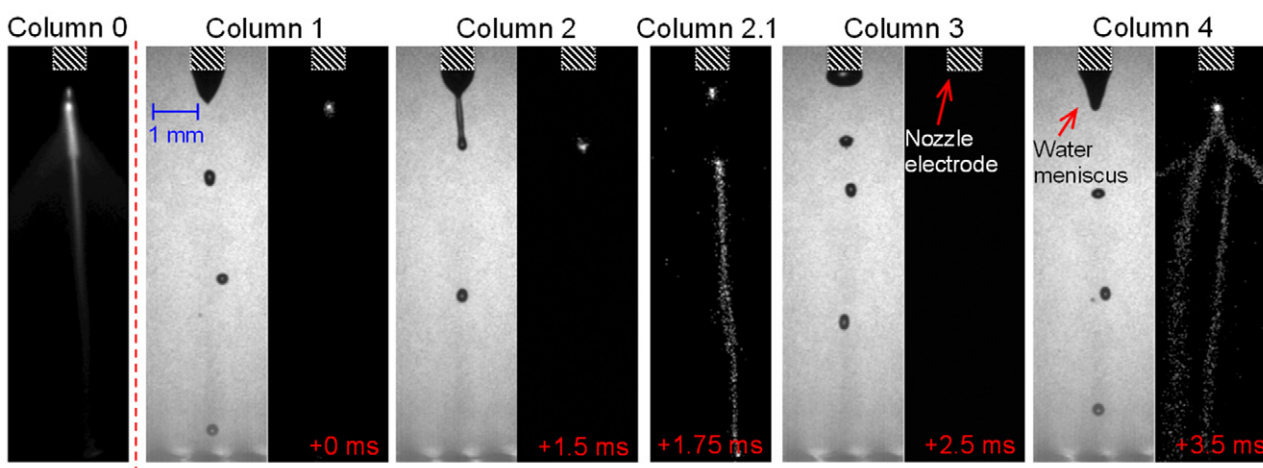


**Figure 11.** iCCD time sequence images of electrospraying of water (illuminated, columns 1–4 with exposure time 10 $\mu$s) with corona discharge (dark, columns 1–4 with exposure time 100 $\mu$s) in spindle mode for water conductivity 4500 $\mu$S cm$^{-1}$, + 6 kV, gap 1 cm, nozzle 0.8 mm o.d. and 0.6 mm i.d. iCCD dark images in column 0 with exposure time 5 s represent an integrated emission over the long period with many droplet formation cycles.

activity on the filament tip and its resultant space charge around the tip are therefore enhanced as the liquid filament proceeds along the gap. Since the filament head with an active corona is surrounded by a strong space charge of ions of the same polarity, the electric field and so the electric pressure on the filament head become more reduced. Under such conditions, the capillary pressure also decreases to equilibrate the reduced electric pressure, and the tip thus becomes more spherical with a surface of larger radius of curvature [28]. Note that despite the fact that this process of propagating the water filament head surrounded by space charge can be intuitively compared to the streamer head propagation, the streamer head propagation is several orders of magnitude faster ($\sim 10^6$ m s$^{-1}$) than the water filament head propagation in our experimental conditions ($\sim 1$ m s$^{-1}$, for our typical water flow rates, based on the iCCD images in figures 9–11). So unlike in the streamer head that propagates extremely fast due to photoionization, and leaves the cloud of positive space charge behind, which enhances the electric field on the streamer head, our water filament propagates very slowly; its head cannot escape the space charge from the positive ions forming around it. Consequently, the positive space charge around the filament head reduces the electric field, thus the electric pressure and the compensating capillary pressure get reduced too, resulting in a more spherical head with a surface of larger radius of curvature.

On the other hand, in poorly conductive liquids the liquid acts more as an insulator and so the electrical resistance of the growing water filament partially suppresses the corona activity. Therefore, the corona ionic space charge is prevented from accumulating near the filament surface, and subsequently the surface electric field of the filament tip is not reduced as much as in the conductive liquids. Therefore, the tip is more pointed with a surface of smaller radius of curvature [28].

After the detachment of the elongated water fragment, and the contraction of the water meniscus back towards the nozzle, the glow corona disappeared (column 3, the dark image is without any bright spots). This may simply be caused by the reduction of the electric field near the nozzle due to the decrease in the water meniscus curvature due to insufficient water volume to form the cone. Additionally, the presence of the droplets under the nozzle could also reduce the field, since they carry charges of the same polarity as the nozzle and weaken the field on it [11, 21]. With the disappearance of corona activity on the meniscus surface, the surface electric field is no longer reduced by the corona space charge and so the enhanced electric field on the water surface of the newly accumulated water droplet starts to deform its surface again, thus reforming a cone.

Finally, after a few ms, a new cone is formed (decreasing the radius of curvature and so increasing the intensity of the electric field), and the filamentary discharge occurs from the cone tip to the ground electrode (column 4). This discharge is similar to the onset streamer in short gaps and is responsible for the generation of the measured current pulses that trigger the iCCD camera (figures 2, 5 and 8). In highly conductive water, filamentary discharge sometimes also occurred from the spherical tip of the elongated water

filament right before its detachment from the nozzle (figure 11, column 2.1). This was not observed in the low conductivity water. The measured current amplitudes of several mA in the filamentary streamer discharge definitely cause a large voltage drop in low conductivity water where the filament represents a resistance of a few M$\Omega$. This resistance, in series with the ballast resistor of 20 M$\Omega$, enables a very short duration of the streamer pulse as the voltage is dropped immediately after the streamer current pulse, and prevents the evolution of the spark breakdown. With higher conductivities, the voltage drop along the filament becomes negligible with respect to the one across the ballast resistor.

The electrospraying event with discharge propagation did not change very much with the increasing voltage within the studied range, and so the image sequences for other voltage values are not shown here. However, with higher voltages, the glow corona was always present on the water meniscus, even after the detachment of elongated water fragment from the nozzle. This led to the formation of a water cone that was not as sharp as in the lower voltage shown in column 1 of figures 9–11, but was more rounded. A filamentary discharge eventually occurred from this rounded cone, too.

According to the theory of the streamer and glow corona generation from metal surface, extensively elaborated and described elsewhere, e.g. in [35, 37], the onset streamer is always present before the start of a positive glow corona. Obviously, the same phenomenon can be observed in the experiment with electrospray. The difference in our case is that the surface is a liquid and it oscillates. Thus, this corona discharge is unstable and depends on the water meniscus propagation. On the other hand, the presence of a discharge generating a space charge in the vicinity of the water meniscus causes the reduction of the electric field in this area. This can disrupt the balance between the electric and the capillary forces determining the water filament shape, propagation, and stability [16, 28].

These results show the reciprocal character of intermittent electrospraying of water with the presence of corona discharge, where both phenomena affect each other. Another interesting phenomenon can be seen from figures 9–11 when comparing the dark images with long exposure time 5 s (column 0) and short exposure time 100 $\mu$s (columns 1–4). One can notice that the small bright streak under the nozzle in column 0 (few mm long) is in fact created by the periodical down–up movement of the water filament with the glow corona discharge on its tip (integrated over a long time). The light emission of the onset streamer is negligible in these long exposure images due to the short streamer duration and its relatively low repetition frequency.

## 4. Conclusions

The fast high-speed (HS) camera and iCCD camera imaging combined with oscilloscopic current pulse measurements were used to investigate the effect of electrospraying of water in combination with positive corona discharge in a relatively short gap (1 cm). This combination of non-thermal air plasma with water spray is a promising method for water decontamination

since it enhances the mass transfer of active plasma species into water. Our objective was to identify the spraying modes typical for water of various conductivities and to investigate the discharge propagation with the presence of the electrospray.

With the increasing voltage is applied on the spraying nozzle, several intermittent modes of electrospraying mentioned in the literature were observed: the dripping mode at low voltages was followed by the spindle mode, which was more significant with elongated filaments for deionized water with low conductivity. At a short range of voltages, an oscillating-spindle mode was also observed. The microdripping mode was not present, probably due to the high water flow rates. Since the experiments were conducted in ambient air with water, which is a liquid with high surface tension, all kinds of cone–jet modes were not established. The necessary voltage for electrospraying in cone–jet mode was higher than the electric breakdown threshold of the surrounding gas and a disruptive filamentary discharge phenomena occurred, which prevented these modes. Our major findings can be summarized as follows:

1 Considering the water decontamination applications, the estimated average time of flight and the dimensions of the sprayed water droplets between the electrodes were calculated. In the spindle mode with deionized water, the droplet flight time was relatively short (from 100 to 2.5 ms) and droplets sizes were relatively small (from less than 10 to 250 $\mu$m in diameter). The characteristic droplets sizes became larger (from 190 to 280 $\mu$m in diameter) and the time of flight became longer (from 2.7 ms to 6.3 ms) with higher water conductivities.

2 The observed modes of electrospraying had an intermittent character with a characteristic mode repetition frequency of a few hundreds of Hz, as measured from the fast image sequences. In most cases, especially for lower voltages, the repetition frequency was relatively stable. Under these conditions, this frequency agreed well with the frequency of measured current pulses.

3 Parallel measurements by HS camera and oscilloscope provided evidence that there was a clear correlation between the intermittent electrospray and the corona discharge. The current pulses were generated by a streamer corona discharge occurring from the sharp Taylor cone tip. The generation of this discharge from the water cone depended on the repetitive process of cone formation, as supported by the measurements of mode repetition frequency matching with the frequency of the current pulses. After the streamer, a positive glow corona discharge was established on the water filament tip. The glow corona discharge generation and its propagation from the stressed electrode depended on the water meniscus propagation and its elongation. On the other hand, the presence of the discharge and its resultant space charge influenced the electrospray phenomenon and water filament tip curvature by disrupting the balance between the electric and the capillary forces. These phenomena were also influenced by the water conductivity. The results showed the reciprocal influence of the intermittent electrospray of water and the corona discharge.

## References

[1] Zeleny J 1914 *The Phys. Rev.* **3** 69–91
[2] Zeleny J 1917 *The Phys. Rev.* **10** 1–8
[3] Taylor G 1964 *Proc. R. Soc. Lond.* A **280** 383–97
[4] Smith D P H 1986 *IEEE Trans. Industry Appl.* **1A-22** 527–35
[5] Hayati I, Bailey A I and Tadros Th F 1987 *J. Colloid Interface Sci.* **117** 205–21
[6] Hayati I, Bailey A I and Tadros Th F 1987 *J. Colloid Interface Sci* **117** 222–30
[7] Bailey A G 1988 *Electrostatic Spraying of Liquids* (New York: Wiley)
[8] Cloupeau M and Prunet-Foch B 1990 *J. Electrostat.* **25** 165–84
[9] Hartman R P A, Borra J P, Brunner D J, Marijnissen J C M and Scarlett B 1999 *J. Electrostat.* **47** 143–70
[10] Lim L K, Hua J, Wang C H and Smith K A 2011 *AIChE J.* **57** 57–78
[11] Hartman R P A, Brunner D J, Camelot D M A, Marijnissen J C M and Scarlett B 2000 *J. Aerosol Sci.* **31** 65-95
[12] Rayleigh L 1882 *Phil. Mag.* **14** 184–6
[13] Li K Y, Tu H and Ray A K 2005 *Langmuir* **21** 3786-94
[14] Borra J P, Ehouarn P and Boulaud D 2004 *J. Aerosol Sci.* **35** 1313–32
[15] López-Herrera J M, Barrero A, Boucard A, Loscertales I G and Márquez M 2004 *J. Am. Soc. Mass Spectrom.* **15** 253–9
[16] Cloupeau M and Prunet-Foch B 1989 *J. Electrostat.* **22** 135–59
[17] Chen D R, Pui D Y H and Kaufman S L 1995 *J. Aerosol Sci.* **26** 963–77
[18] Jaworek A 2007 *Powder Technol.* **176** 18–36
[19] Tang K and Gomez A 1995 *J. Colloid Interface Sci.* **175** 326–32
[20] Cloupeau M and Prunet-Foch B 1994 *J. Aerosol Sci.* **25** 1021–36
[21] Jaworek A and Krupa A 1999 *J. Aerosol Sci.* **30** 873–93
[22] Machala Z, Chládeková L and Pelach M 2010 *J. Phys. D: Appl. Phys.* **43** 222001
[23] Machala Z, Tarabová B, Hensel K, Spetlíková E, Šikurová L and Lukeš P 2013 *Plasma Process. Polym.* **10** 649–59
[24] Koval'ová Z, Tarabová K, Hensel K and Machala Z 2013 *Eur. Phys. J. Appl. Phys.* **61** 24306
[25] Zeleny J 1920 *Phys. Rev.* **16** 102–25
[26] English W N 1948 *Phys. Rev.* **74** 179–89
[27] Dawson G A 1970 *J. Geophys. Res.* **75** 2153–8
[28] Kuroda S and Horiuchi T 1984 *Japan. J. Appl. Phys.* **23** 1598–607
[29] Cloupeau M 1994 *J. Aerosol Sci.* **25** 1143–57
[30] Jaworek A and Krupa A 1997 *J. Electrostat.* **40–41** 173–8
[31] Jaworek A, Czech T, Rajch E and Lackowski M 2005 *J. Electrostat.* **63** 635–41
[32] Shirai N, Sekine R, Uchida S and Tochikubo F 2014 *Japan. J. Appl. Phys.* **53** 026001
[33] Kim H H, Kim J H and Ogata A 2011 *J. Aerosol Sci.* **42** 249–63
[34] Pongrác B, Kim H H, Negishi N and Machala Z 2014 Influence of water conductivity on the electrospray with dc corona discharge—optical visualization approach *Eur. Phys. J.* D **68** at press
[35] Morrow R and Lowke J J 1997 *J. Phys. D: Appl. Phys.* **30** 614–27
[36] Giao T N and Jordan J B 1968 *IEEE Trans. Power Apparatus Syst.* **87** 1207–15
[37] Morrow R 1997 *J. Phys. D: Appl. Phys.* **30** 3099–114